Monte Carlo modeling of electron backscattering from carbon nanotube forests

M. K. Alam, P. Yaghoobi, and A. Nojeh[a)]
Department of Electrical and Computer Engineering, The University of British Columbia, Vancouver, British Columbia V6T 1Z4, Canada

(Received 8 July 2010; accepted 11 October 2010; published 9 November 2010)

The authors present a new Monte Carlo tool capable of simulating electron trajectories in nanotube forests, taking into account the underlying nanoscale nature of the material. The scattering angle distribution is adaptively modified at each step of the simulation according to the local environment (how the nanotubes are positioned, their diameters, and internanotube distances). This provides additional degrees of freedom in the Monte Carlo simulation that are directly related to the internal structure of the nanotube forest, allowing the model to closely match experimental data. © *2010 American Vacuum Society.* [DOI: 10.1116/1.3511506]

I. INTRODUCTION

The interaction of electron beams with solids has been studied for a long time because of interest in both the fundamentals of the interaction mechanisms and predicting electron yield[1–6] as well as making vacuum devices such as electron multipliers and detectors.[7,8] Carbon nanotubes (CNTs), with their interesting electrical, mechanical, thermal, and optical properties, are promising candidates for many applications,[9] in particular, in the areas of electronics and free-electron devices. Given the nanoscale and hollow structure of CNTs, their interaction with electron beams and imaging mechanisms in electron microscopy are expected to be quite different from those of bulk materials.[10–17] Electron energy loss spectra in carbon nanostructures have been calculated by considering the polarizability of each carbon atom in the structure.[18] A model for calculating the dielectric response function for CNTs has also been proposed and used to calculate electron inelastic mean free paths and average energy transfer for single inelastic scattering.[19,20] Experimental works on the imaging mechanisms of CNTs (Refs. 10–14) and high electron yield from coated multiwalled nanotube (MWNT) forests have been reported.[15–17] The interaction of electrons with CNTs has also been studied using first-principles simulations.[21,22] However, to the best of our knowledge, there is no report on modeling backscattered or secondary electron yield from CNTs or CNT-based structures such as forests of vertically aligned CNTs.

The Monte Carlo method has been used extensively for the simulation of electron trajectories and yield from bulk materials.[6,23] The material is implemented as a homogeneous, isotropic structure for the purposes of these Monte Carlo simulations. However, a CNT forest is a semiregular array of a large number of substructures (individual CNTs) with empty spaces in between, making it a nonhomogeneous and anisotropic structure. One would expect that such a structure cannot be treated in the same manner as a regular bulk material in a physically meaningful way. Recently, we reported unusual electron backscattering and secondary electron emission behavior from CNT forests.[24] This was attributed to the porous nature of the structure that leads to an unusually high electron penetration range (distance traveled by the primary electron inside a specimen before it loses all of its kinetic energy). Here, we present a semiempirical model for electron backscattering from CNT forests using physically meaningful empirical parameters. These parameters bring additional degrees of freedom into the simulation that can be directly correlated with the internal structure of the forests. We also present the results of Monte Carlo simulations based on this model and compare the results with our previously published[24] and new experimental data.

II. FABRICATION AND EXPERIMENTS

The fabrication of CNT forests and details of experimental measurements have been discussed elsewhere.[24] In brief, CNT forests were fabricated using standard microfabrication for patterning catalyst and chemical vapor deposition (CVD) for the growth of CNTs. Al and Fe of 10 and 2 nm, respectively, in thickness were used as catalyst to grow vertically aligned, millimeter-long MWNT forests. The backscattering yield was measured from the CNT forests in a scanning electron microscope for a wide range of primary beam energies.[24]

III. MODEL

Our model is based on the widely accepted Monte Carlo model by Browning *et al.*[25] In this model, the step length of an electron is obtained from[6,23]

$$s = \lambda \ln R, \tag{1}$$

where s is the step length (which follows a Poisson distribution), λ is the mean free path (MFP), and R is a uniform random number between 0 and 1. MFP (λ) can be estimated from the density of the target and its scattering cross section.[6]

The scattering angle (θ) is estimated from a fitted Mott differential cross section. The fitted cross section is com-

[a)]Author to whom correspondence should be addressed; electronic mail: anojeh@ece.ubc.ca

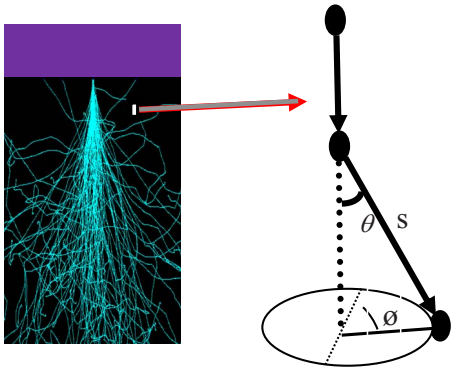

(a) (b)

FIG. 1. (Color online) (a) Electron trajectories in a typical Monte Carlo simulation showing the randomness of beam-specimen interaction and (b) one small step in a single trajectory (s=step length, θ=scattering angle, and ϕ=azimuthal angle).

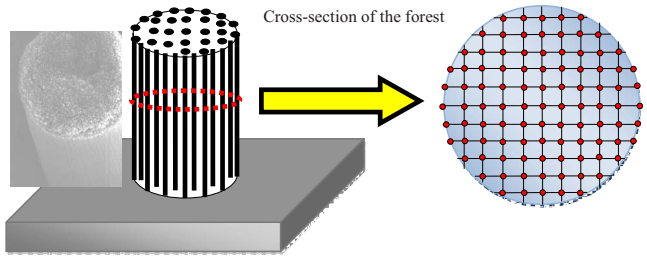

(a) (b)

FIG. 2. (Color online) (a) Micrograph and schematic of a circularly patterned CNT forest and (b) top view of the CNT grid used in Monte Carlo simulations. (CNT diameter and internanotube spacing have been exaggerated in the schematics for clarity.)

posed of two parts: the screened Rutherford and isotropic distributions,[25] which lead to the following forms for scattering angle distribution:

$$\cos\theta = 1 - \frac{2\alpha R}{1+\alpha-R} \quad \text{(Rutherford scattering)}, \tag{2}$$

$$\cos\theta = 1 - 2R \quad \text{(isotropic scattering)}, \tag{3}$$

where α is the screening parameter. Only the screened part of the cross section depends on the screening parameter. For pure bulk material, α is calculated from

$$\alpha = \frac{7\times 10^{-3}}{E}, \tag{4}$$

where E is the incident electron energy in keV.

The azimuthal angle (ϕ) is calculated from a uniform distribution

$$\phi = 2\pi R, \tag{5}$$

Fig. 1 shows typical electron trajectories and a single step of a Monte Carlo simulation for a bulk material. The incident energy at each step is calculated based on the energy loss rate, obtained from

$$\frac{dE}{ds} = -785\frac{\rho Z}{AE}\ln\left(\frac{1.166(E+tJ)}{J}\right) \ \text{eV/Å}, \tag{6}$$

where s is the interaction length [Eq. (1)] in the traveling direction of the primary electron, ρ is the density of the target, Z is the atomic number, A is the atomic weight, E is the incident energy, J is the mean excitation potential,[6,26] and t is an empirical factor, which is usually 0.77 for carbon.[5,6,27]

This method has been extensively used for bulk materials.[28,29] On the other hand, as mentioned earlier, a CNT forest is an array of many individual CNTs (Fig. 2) and may behave differently from a bulk solid. For the purposes of the present work, we defined the forest as a rectangular array of CNTs [Fig. 2(b)], although this does not diminish the generality of the model. Each grid point indicates the center of a CNT in the forest. We estimated the average diameter of the CNTs (10 nm) and the spacing between CNT walls (36 nm) based on transmission electron miscroscopy and experiments on liquid-induced shrinkage of the forests, as reported previously.[24]

Another important parameter is the density of the forests. It is known that backscattering from the surface is not highly sensitive to density.[6] However, the sidewall scattering observed from these forests at high primary beam energies seems to be due to the low density and porous nature of the forests.[24] For a given chirality of nanotubes and number of walls per MWNT, the density can be obtained from

$$\text{density}(\rho) = N_{\text{TA}} \times N_{\text{AL}} \times m_{\text{l}}, \tag{7}$$

where N_{TA} is the number of CNTs per unit area, N_{AL} is the number of atoms along the CNT axis per unit length of the CNT, and m_{l} is the mass of a carbon atom. Due to the low level of control in existing fabrication processes, not only do these parameters vary from forest to forest, even within one forest, the CNTs will have different chiralities and numbers of walls. The density of MWNT forests can be estimated to be on the order of 10^{-2} g/cm^3 for an internanotube spacing of ~36 nm (distance between the outer walls of adjacent nanotubes) depending on the number of walls and chiralities. For example, for a four-wall MWNT including chiralities of (95, 0), (104, 0), (113, 0), and (122, 0), the density is 0.0296 g/cm^3. Futaba *et al.* estimated the density of their single-walled CNT forests to be on the order of 0.029 g/cm^3 (calculated for an inter-CNT spacing of 16.4 nm and CNT diameter of 2.8 nm).[30] Given these variations, we kept the density as an empirical parameter to be obtained by fitting to the experimental data.

Next, we turn to the treatment of the scattering angle, which constitutes the main difference between the proposed model for CNT forests and the bulk model. Figure 3 shows a typical distribution of scattering angles (obtained from 10 000 scattering events) and its dependence on the screening parameter (α). A low value of α indicates a higher probability of low angle scattering, and vice versa. Given a fixed value of α for the simulation, the scattering angle probability distribution depends only on the incident energy. For CNT forests, which consist of individual CNTs with empty spaces

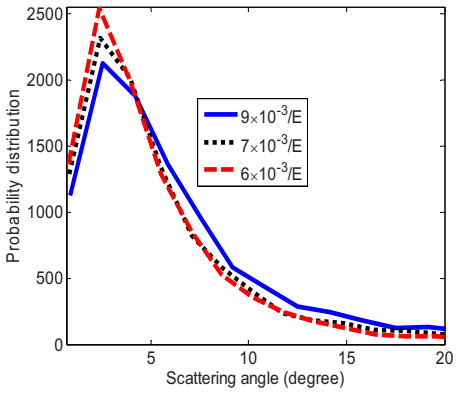

FIG. 3. (Color online) Typical distribution of the scattering angle (for 10 000 scattering events with 100 energy bins) and change in the distribution with the change of screening parameter.

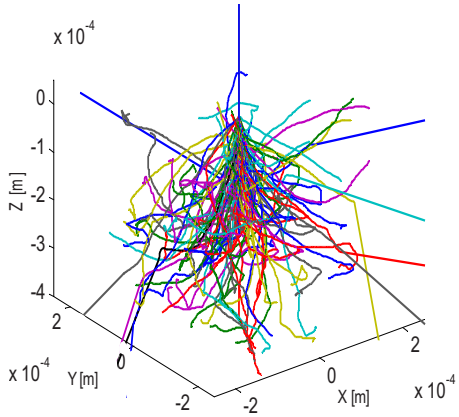

FIG. 5. (Color online) 100 electron trajectories (primary energy is 20 keV) through a 500-μm-diameter CNT forest, obtained using the described Monte Carlo program.

in between, the idea is to adaptively shift the scattering angle distribution at each step of the simulation based on the position of the primary electron. The rationale is that, for a given step of the Monte Carlo simulation, larger scattering angles are to be favored if an electron scatters from the wall (Fig. 4, R-2) of a CNT compared to when it scatters in the empty spaces between CNTs (Fig. 4, R-3) or inside a CNT (Fig. 4, R-1). One way to achieve the required modification may be to adaptively vary the width of the scattering angle distribution by adopting a higher value for the screening parameter for steps where the primary electron ends up on the CNT wall (Fig. 4, R-2) and a lower value when the scattering site is far from the CNT wall (R-1 and R-3 in Fig. 4). However, this approach still would not take the anisotropic nature of the forest into account. Therefore, in the proposed model, rather than changing the width of the scattering angle distribution, we shifted the center of the distribution according to the location of the scattering site in each step. To implement this, the effective CNT shell thickness (Fig. 4) was introduced as an empirical parameter.

The position of the primary electron relative to the surrounding CNTs was checked at each step of the simulation. Note that we did not need to save the positions of all the nanotubes in the memory, which would have been prohibitive due to the extremely high number of nanotubes forming

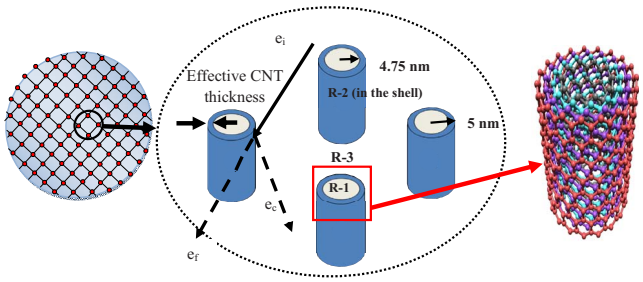

FIG. 4. (Color online) Schematic representation of the CNT grid (R-1 =hollow region enclosed by the shell, R-2=in the shell, and R-3=outside the shell) and proposed change in scattering angle distribution for the screened part of the fitted differential cross section in a particular step of the simulation, where the scattering site falls within a CNT shell (R-2).

the forest. Instead, having them on a regular grid allowed us to easily determine the relative position of the electron and the nanotubes in its close proximity at every step. This made the simulator memory-efficient and allowed the simulation of macroscopically sized forests in a reasonable time on a regular computer. If the primary electron fell within the shell of a CNT (Fig. 4, R-2), the center of the scattering angle distribution (the direction of forward movement) was changed according to the elastic collision law (mirror reflection) to favor large angle scattering. This is illustrated in Fig. 4, where the direction of forward movement is shifted from the e_f direction to the e_c direction. In this way, the inhomogeneous and anisotropic nature of CNT forests were incorporated in the simulation and the empirical parameters were found by fitting to experimental data. Note that in reality, the nanotubes in the forest, although overall highly aligned, are not perfectly straight and have wiggle and physical entanglement with each other. Since the exact geometry of all the nanotubes in the forest cannot be known, we include this effect by assuming that the (straight) nanotubes are in an effective background space (R-1 and R-3 in Fig. 4), where electrons do scatter, although without shifting the center of the scattering angle distribution. In addition, a portion of the sidewall scattered electrons hit the substrate. Hence, the substrate was also included in the simulation and treated with the standard bulk model.[25]

IV. RESULTS AND DISCUSSION

Figure 5 shows 100 electron trajectories simulated by our Monte Carlo simulator at a primary electron energy of 20 keV. The simulator was implemented in MATLAB. The straight lines at the end of the trajectories indicate that electrons are escaping from the surface or side of the forest. As can be seen, sidewall escape is the major source of backscattered electrons at high energies as was previously reported in our experimental work.[24]

Figures 6 and 7 show experimental data for CNT forests with diameters of 500 and 200 μm, respectively, and the corresponding simulation results using our proposed model.

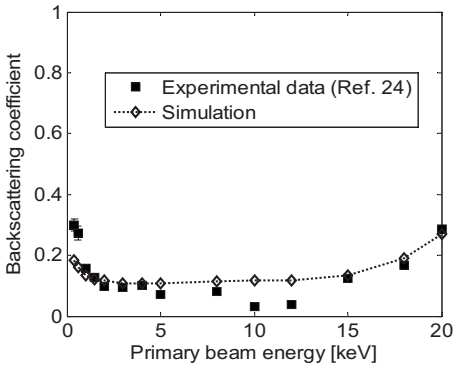

FIG. 6. Comparison of experimental and simulation results for the electron backscattering coefficient from 500-μm-diameter CNT forest.

TABLE I. List of simulation parameters.

Parameters	Value
Diameter of the CNT[a] (nm)	10
CNT spacing[a] (nm)	36
Effective CNT thickness	5% of the CNT radius (0.25 nm)
Screening parameter	$\frac{6\times10^{-3}}{E[\mathrm{keV}]}$
Total trajectories	10 000
Density of the forest (g/cm^3)	0.019 for 500-μm-diameter forest and 0.0356 for 200-μm-diameter forest
Beam direction	Perpendicular to the top surface

[a]Reference 24.

Most of the error bars in the experimental data are masked by the curve markers. Trajectories of 10 000 electrons were simulated at each primary electron energy in all the simulations. The experimental data set shown in Fig. 6 was initially used for finding the empirical parameters. The same values of screening parameter and shell thickness were then used in order to simulate the data of Fig. 7; however, a new value of density (Table I) was found to improve the fit, particularly in the high-energy region. The detailed procedure for finding the empirical parameters is discussed in the Appendix. The structural and empirical parameters used for fitting the simulations to experiments are summarized in Table I.

As can be seen, the simulated results are in good agreement with our measured data. The rms error was found to be less than 0.05 (0.046 for the 500-μm-diameter forest and 0.0139 for the 200-μm-diameter forest). The large angle scatterings from CNT walls in our model were taken care of by the shift of the distribution. Therefore, the lower value of the screening parameter found in our simulation does not contradict the increased probability of large angle scattering from MWNT walls.

At this point, it is also important to try to match the experimental data using the traditional bulk model. The result is shown in Fig. 8 for the 500-μm-diameter forest. In order to obtain a good fit with experimental data, the screening parameter needed to be increased to 9×10^{-3}/E. This indicates an overall higher probability of large angle scattering for the forest compared to bulk solids.

This result could be due to the fact that the traveling electron now encounters many boundaries (the CNT walls) throughout the structure, which might deflect it significantly more than when the electron travels within a homogeneous material. In addition, electron delocalization along the nanotubes could affect screening and, therefore, the scattering angle distribution. It is thus seen that the bulk model, using this new value of the screening parameter, is quite successful at reproducing the experimental data. The rms error for the predictions of the adjusted bulk model [0.0442 for the 500-μm-diameter forest and 0.0242 for the 200-μm-diameter forest (results not shown here)] was found to be similar to or slightly higher than that for the simulations performed using the proposed model for the same set of experimental data. Therefore, a question might arise regarding the possible advantages of a more elaborate model, such as the one presented here. To address this issue, one has to consider the fact that when the forest diameter is significantly larger than the mean free path of the electrons, which is the case in the experimental data used here, each electron undergoes many scatterings. Although due to the anisotropic nature of the structure, some of these scatterings will be to one side of a particular CNT and some to the other, the effect

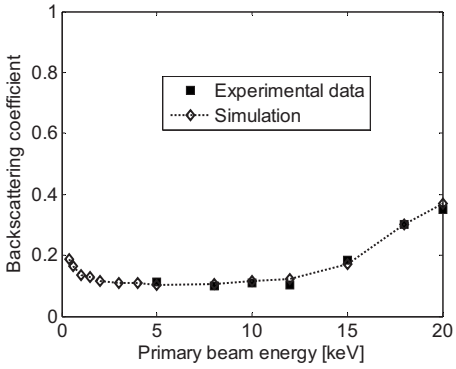

FIG. 7. Comparison of experimental and simulation results for the electron backscattering coefficient from 200-μm-diameter CNT forest.

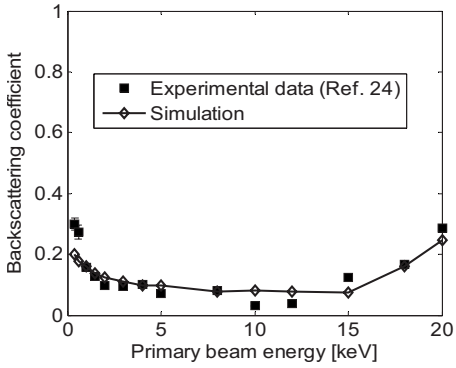

FIG. 8. Comparison of experimental and simulation results for the electron backscattering coefficient from 500-μm-diameter CNT forest using the adjusted bulk model.

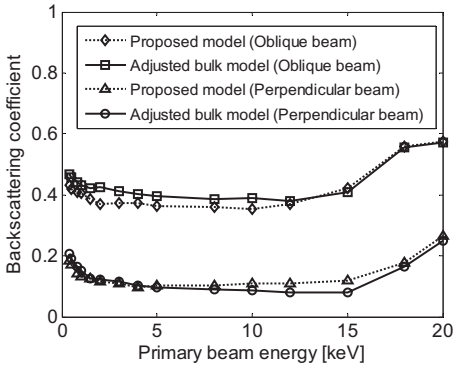

FIG. 9. Comparison of the proposed and adjusted bulk model for the predicted electron backscattering coefficient from the 500-μm-diameter CNT forest using the extracted empirical parameters. The direction cosines for oblique incidence are $\cos(x)=0$, $\cos(y)=-0.9367$, and $\cos(z)=0.3501$.

is averaged out over many scattering events and results in an effective increase in the probability of high angle scattering in all directions. This is why the bulk model works for this system, albeit with a larger screening parameter than usual. However, the situation might be different if the microscopic details of the interaction of each particular electron with the system, such as the preferred directions of escape from a given region within the forest, are of interest. For instance, we speculate that effects similar to channeling of particles in crystals might take place in the CNT forest, the study of which will require a model that deals with the internal, nanoscale structure of the forest. The model proposed here is a first step in this direction.

In addition, our experimental data so far pertain to a case with cylindrical symmetry around the forest axis as the primary electrons impinge on the top surface of the forest perpendicular to it. The situation may be different when this symmetry is broken, such as when the primary beam is incident on the surface of the forest at an oblique angle. It was observed that the proposed model would deviate noticeably from the adjusted bulk model for an obliquely incident beam (keeping all the parameters the same as before for both models).

Figure 9 shows a comparison of the predictions of our proposed model with those of the adjusted bulk model for an oblique beam. It is seen that the adjusted bulk model predicts a higher backscattering yield than the proposed model for primary energies up to ~15 keV for an obliquely incident beam, whereas it predicts otherwise for perpendicular incidence above 5 keV.

V. SUMMARY

A model for electron backscattering from CNT forests taking into account the internal nanoscale nature of the forest structure was proposed and parametrized using experimental data. It was also seen that the traditional bulk model could generate similar results (although with a new value of the screening parameter). However, if the microscopic aspects of the electron movement through the forest and phenomena similar to channeling are of interest, the bulk model cannot provide an adequate representation and more elaborate models, taking the porous forest structure into account, are needed. The model proposed here is a first step in this direction. These results may have important implications in the study of the interaction of electron beams with nanostructures, such as for modeling secondary electron emission or x-ray microanalysis from CNT-based structures.

ACKNOWLEDGMENTS

The authors acknowledge the financial support from the Natural Sciences and Engineering Research Council (Grant Nos. 341629-07 and 361503-09), the Canada Foundation for Innovation (Grant No. 13271), and the British Columbia Knowledge Development Fund (BCKDF). M.K.A. also acknowledges partial support from a University of British Columbia Graduate Fellowship. P.Y. also acknowledges additional support from the University of British Columbia.

APPENDIX

The empirical fit procedure is shown in the flow diagram (Fig. 10). To find an optimal method, we first simulated the distinct effects of each empirical parameter on the backscattering coefficient of a 500-μm-diameter forest. It was observed that the screening parameter affects the entire energy range. The backscattering yield increases with the increase of the screening parameter and vice versa. The reason is that large angle scattering increases with the increase of the screening parameter (see Fig. 3 and Sec. IV). It was also seen that a smaller effective CNT thickness (i.e., 5% of the CNT radius) produces less fluctuation, which is more realistic (Fig. 6) compared to a higher value of the CNT thickness. It is also known that surface backscattering is not highly sensitive to the density of a material[6] (also confirmed by our

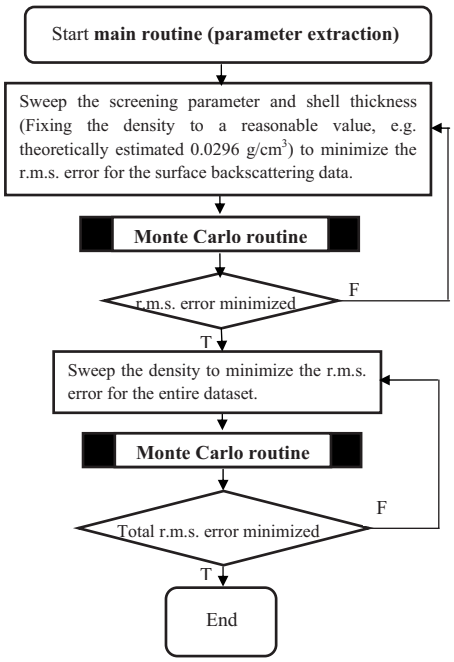

FIG. 10. Flow diagram of the empirical fit routine.

simulations). Sidewall scattering (which affects the yield at high primary energies) increases with the decrease of the density, while surface backscattering remains almost the same. Therefore, we started the empirical fit routine to match the surface backscattering data (Fig. 6 before 12 keV) by sweeping the screening parameter and shell thickness while keeping the density fixed at a reasonable value such as the theoretically estimated value ($0.0296\ \mathrm{g/cm^3}$).

The rms error was minimized for the surface backscattering data (Fig. 6 before 12 keV) with respect to the screening parameter and effective shell thickness. Once these two parameters were known, the density was adjusted in order to improve the fit (minimize the rms error), in particular, for the high-energy backscattering data (Fig. 6 beyond 12 keV). At this step, the entire data set was taken into consideration to minimize the rms error. Thus, the empirical parameters were estimated from the data set for the 500-μm-diameter forest (Fig. 6).

The same set of parameters (screening parameter, shell thickness, and density) was then used to predict the backscattered yield of the 200-μm-diameter forest. It was found that the experimental surface backscattering data (Fig. 7 before 10 keV) fit the predicted results very well. This indicates that the extracted screening parameter and the effective CNT thickness, derived from the 500-μm-diameter forest, are also applicable to other structures. However, we needed to change the density to $0.0356\ \mathrm{g/cm^3}$ (corresponding to a difference of $\sim$26% in the average distance between the CNTs assuming everything else remains the same) to improve the fit for the sidewall scattering part of the data (Fig. 7 after 10 keV). Note that our two forests with the different diameters were grown during different CVD runs. Due to the current limitations of nanotube fabrication, the forest density could vary from growth to growth depending on the uniformity and size of the catalyst particles created during the annealing of the catalyst films. It also depends on the ambient pressure, gas flow rate, and growth dynamics. Therefore, a 26% change in the nanotube spacing or a change in the chirality (which also contributes to the density) is very reasonable in the CVD growth of nanotube forests.

[1] K. G. McKay, *Secondary Electron Emission: Recent Advances in Electronics* (Academic, New York, 1948), Vol. 1, p. 65.
[2] E. M. Baroody, Phys. Rev. **78**, 780 (1950).
[3] A. J. Dekker, Phys. Rev. Lett. **4**, 55 (1960).
[4] C. G. H. Walker, M. M. El-Gomati, A. M. D. Assa'd, and M. Zadražil, Scanning **30**, 365 (2008).
[5] L. Reimer, *Scanning Electron Microscopy: Physics of Image Formation and Microanalysis* (Springer, Berlin, 1998), Vol. 45, p. 135.
[6] D. C. Joy, *Monte Carlo Modeling for Electron Microscopy and Microanalysis* (Oxford University Press, New York, 1995), Vol. 9, p. 25.
[7] S. Pendyala, J. W. McGowan, P. H. R. Orth, and P. W. Zitzewitz, Rev. Sci. Instrum. **45**, 1347 (1974).
[8] D. Shapira, T. A. Lewis, L. D. Hulett, Jr., and Z. Ciao, Nucl. Instrum. Methods Phys. Res. A **449**, 396 (2000).
[9] R. H. Baughman, A. A. Zakhidov, and W. A. de Heer, Science **297**, 787 (2002).
[10] T. Brintlinger, Y.-F. Chen, T. Dürkop, E. Cobas, M. S. Fuhrer, J. D. Barry, and J. Melngailis, Appl. Phys. Lett. **81**, 2454 (2002).
[11] A. Nojeh, W.-K. Wong, A. W. Baum, R. F. W. Pease, and H. Dai, Appl. Phys. Lett. **85**, 112 (2004).
[12] P. Finnie, K. Kaminska, Y. Homma, D. G. Austing, and J. Lefebvre, Nanotechnology **19**, 335202 (2008).
[13] Y. Homma, S. Suzuki, Y. Kobayashi, M. Nagase, and D. Takagi, Appl. Phys. Lett. **84**, 1750 (2004).
[14] W. K. Wong, A. Nojeh, and R. F. W. Pease, Scanning **28**, 219 (2006).
[15] W. Yi *et al.*, J. Appl. Phys. **89**, 4091 (2001).
[16] W. S. Kim *et al.*, Appl. Phys. Lett. **81**, 1098 (2002).
[17] J. Lee, J. Park, K. Sim, and W. Yi, J. Vac. Sci. Technol. B **27**, 626 (2009).
[18] A. Rivacoba and F. J. G. de Abajo, Phys. Rev. B **67**, 085414 (2003).
[19] I. Kyriakou, D. Emfietzoglou, R. Garcia-Molina, I. Abril, and K. Kostarelos, Appl. Phys. Lett. **94**, 263113 (2009).
[20] D. Emfietzoglou, I. Kyriakou, R. Garcia-Molina, I. Abril, and K. Kostarelos, J. Appl. Phys. **108**, 054312 (2010).
[21] A. Nojeh, B. Shan, K. Cho, and R. F. W. Pease, Phys. Rev. Lett. **96**, 056802 (2006).
[22] M. K. Alam, S. P. Eslami, and A. Nojeh, Physica E (Amsterdam) **42**, 124 (2009).
[23] M. Dapor, *Electron-Beam Interactions with Solids: Application of Monte Carlo Method to Electron Scattering Problems* (Springer, New York, 2003), Vol. 186, p. 69.
[24] M. K. Alam, P. Yaghoobi, and A. Nojeh, Scanning **31**, 221 (2009).
[25] R. Browning, T. Z. Li, B. Chui, J. Ye, R. F. W. Pease, Z. Czyzewski, and D. C. Joy, Scanning **17**, 250 (1995).
[26] W. R. Leo, *Techniques for Nuclear and Particle Physics Experiments: A How To Approach* (Springer, New York, 2005), Vol. 1, p. 24.
[27] D. C. Joy and S. Luo, Scanning **11**, 176 (1989).
[28] N. W. M. Ritchie, Surf. Interface Anal. **37**, 1006 (2005).
[29] D. Drouin, A. R. Couture, D. Joly, X. Tastet, V. Aimez, and R. Gauvin, Scanning **29**, 92 (2007).
[30] D. N. Futaba *et al.*, Nature Mater. **5**, 987 (2006).